PAPER

Large-scale single-cell encapsulation in microgels through metastable droplet-templating combined with microfluidic-integration

View the article online for updates and enhancements.

Biofabrication

PAPER

Large-scale single-cell encapsulation in microgels through metastable droplet-templating combined with microfluidic-integration

Haoyue Zhang[1,7], Liyuan Zhang[2,7], Chuanfeng An[1,3,4,7], Yang Zhang[5], Fei Shao[1], Yijie Gao[6], Yonghao Zhang[1], Hanting Li[1], Yujie Zhang[1], Changle Ren[6], Kai Sun[1], Wei He[1], Fang Cheng[1], Huanan Wang[1,*] (ID) and David A Weitz[2]

1 State Key Laboratory of Fine Chemicals, School of Bioengineering, Dalian University of Technology, Dalian, 116024, People's Republic of China
2 John A. Paulson School of Engineering and Applied Sciences, Harvard University, Cambridge, MA, 02138, United States of America
3 Central Laboratory, Longgang District People's Hospital of Shenzhen & The Second Affiliated Hospital of The Chinese University of Hong Kong, Shenzhen 518172, People's Republic of China
4 Guangdong Key Laboratory for Biomedical Measurements and Ultrasound Imaging, School of Biomedical Engineering, Health Science Center, Shenzhen University, Shenzhen 518060, People's Republic of China
5 Department of Biomedical Engineering, Shenzhen University, Shenzhen, 518037, People's Republic of China
6 Department of Joint Surgery, Dalian Municipal Central Hospital Affiliated of Dalian Medical University, Dalian, 116024, People's Republic of China
7 These authors have contributed equally to this work.
* Author to whom any correspondence should be addressed.

E-mail: huananwang@dlut.edu.cn

Abstract

Current techniques for the generation of cell-laden microgels are limited by numerous challenges, including poorly uncontrolled batch-to-batch variations, processes that are both labor- and time-consuming, the high expense of devices and reagents, and low production rates; this hampers the translation of laboratory findings to clinical applications. To address these challenges, we develop a droplet-based microfluidic strategy based on metastable droplet-templating and microchannel integration for the substantial large-scale production of single cell-laden alginate microgels. Specifically, we present a continuous processing method for microgel generation by introducing amphiphilic perfluoronated alcohols to obtain metastable emulsion droplets as sacrificial templates. In addition, to adapt to the metastable emulsion system, integrated microfluidic chips containing 80 drop-maker units are designed and optimized based on the computational fluid dynamics simulation. This strategy allows single cell encapsulation in microgels at a maximum production rate of 10 ml h^{-1} of cell suspension while retaining cell viability and functionality. These results represent a significant advance toward using cell-laden microgels for clinical-relevant applications, including cell therapy, tissue regeneration and 3D bioprinting.

1. Introduction

Encapsulating living cells in miniaturized hydrogel has attracted increasing attention in tissue engineering, controlled delivery, and cell therapy due to their superior properties over monolithic hydrogels, including highly efficient mass exchange [1], high responsiveness to external stimuli, minimal invasive administration approach, and controllable morphological and mechanical properties [2]. Specifically, these cell-laden microgels can serve as building blocks to be bottom-up assembled into highly cellularized tissue mimics, which protect encapsulated cells from rapid immune clearance; they can also provide a physiologically relevant microenvironment as the artificial extracellular matrix (ECM) to support cell functionalities [3–6]. The use of these cell-laden microgels can potentially lead to a paradigm shift in

regenerative medicine [4, 7–11]. However, decades of persistent efforts show limited success in clinically relevant applications of cell-laden microgels [12, 13], due to the essential challenge of realizing massive, large-scale cell manipulation and encapsulation [14].

Recent progress in miniaturization techniques for the preparation of cell-laden microgels using flow lithography [15, 16] or micromolding [17] has shown potential for enhancing the scalability of cell-laden microgel production. These techniques, however, are still fundamentally limited by their low throughput, batch-to-batch differences, and high cost [18]. Alternatively, droplet-based microfluidic approaches, which enable continuous generation of monodisperse droplets via the precise control of immiscible multiphase flows, have recently emerged as a promising and cost-effective strategy for continuously microgel production [19]. These approaches allow precise control of droplet/particle size distribution and high encapsulation efficiency for single cells [20]. Extensive efforts have been made to develop microfluidic strategies for the large-scale production of droplet/particles under different droplet formation mechanisms, such as continuously splitting dispersed phase into droplets through post-array [21], or parallelizing numerous drop-maker units (DMUs) on one microfluidic chip [22–27]. The largest yield reported so far is 2.09 l h^{-1}, which integrates 10 000 DMUs on a glass-based microfluidic chip produced by deep reactive ion etching technology [23]. Despite the great progress, these scale-up techniques are not applicable for cell encapsulation in microgels due to the high chance of channel blockage attributed to highly viscous hydrogel precursors [28–35]. Moreover, the long-time exposure of cells to the cytotoxic oil and surfactant before transferring into cell culture medium significantly reduces cell viability [10, 30, 31]. These limitations become pronounced when single cell encapsulation is required since the difficulty in designing and fabricating microchannels with requisite reduced size increases substantially [6, 9, 10, 36, 37]. Moreover, the current throughput of single cell encapsulation using droplet microfluidics is 10^5–10^6 events of encapsulation per hour [9, 10], due to the possibility of channel blockage and the large shear forces upon droplet pinch-off. Strategies of parallelizing multiple microchannels for the increase of throughput only reach a production rate of less than 10^6–10^7 events of encapsulation per hour [30], while still having the problem of compromised viability and long-term functionality of the encapsulated cells. This is far below the basic required dose for typical clinical applications, like tissues reconstruction [9, 32, 35] and cell-based therapies [5, 38], which is 10^8–10^9 cells per dose [38]. Besides, the conventional microfluidic techniques to produce cell-laden microgels typically include emulsification for droplet formation, gelation and retrieve microgels into culture media; these steps prolong the

time of cells in the cytotoxic environment [9, 39]. To increase cell viability, one-step microfluidic generation of cell-laden microgels has been developed, such as utilizing spontaneous dewetting emulsion [9], and water-in-water temporary emulsion [40], to decrease the transition time from the oil phase into aqueous phase [10]. However, these techniques are difficult to introduce into scalable microfluidic applications due to the accumulation of microgels inducing channel blockage in the chip. Moreover, the uneven distribution of flow in each channel results in heterogeneity of microgels. Therefore, it is imperative to develop techniques enabling large-scale production of single cell-laden microgels with controllable preparation parameters and retained cell viability and functionality.

Here, we present a droplet microfluidic strategy for the large-scale production of cell-laden microgels based on metastable emulsion-templating combined with microfluidic integration. We introduce perfluoronated alcohols (PFAs), a class of short-chain amphiphilic molecules, as pseudo-surfactants to generate metastable emulsions as sacrificial templates for cell encapsulation in microgels. This strategy achieves a continuous production of cell-laden microgels by triggering on-chip gelation within the time window between emulsification and de-emulsification to spontaneously extract the microgels from the oil into the aqueous phase. Moreover, we further design an integrated microfluidic chip containing 16–80 DMUs optimized by computational fluid dynamics (CFD) simulation; this chip reaches a production rate of 10 ml cell suspension per hour (figures 1(A) and (B)). We further confirm the retained viability and long-term functionality of encapsulated rat mesenchymal stem cells (MSCs) via *in vitro* cell culture and *in vivo* wound healing model using diabetic rats (figure 1(C)).

2. Results and discussion

2.1. Design principle of continuous generation of cell-laden microgels

Conventional techniques for the microfluidic cell encapsulation typically employ amphiphilic fluorinated surfactants [14] to stabilize the water/fluorinated oil interfaces. These fluorinated surfactants generally consist of a large hydrophilic chains, such as polyethylene glycol (PEG) or polyglycerol [35], and long perfluoronated carbon chains (35–110 carbon atoms) to keep hydrophilic-lipophilic balance favorable for W/O emulsions [35, 41, 42]. However, the resulting emulsion are too stable to be broken, making it difficult to retrieve the encapsulated cargoes for further applications (figure 1D(f)). To break the emulsion, typical methods require an excessive amount of solvent to dilute the surfactants or adding amphiphilic molecules to replace the original stable surfactant [10, 43]. By contrast, PFAs are typically comprised of a short alcohol chain
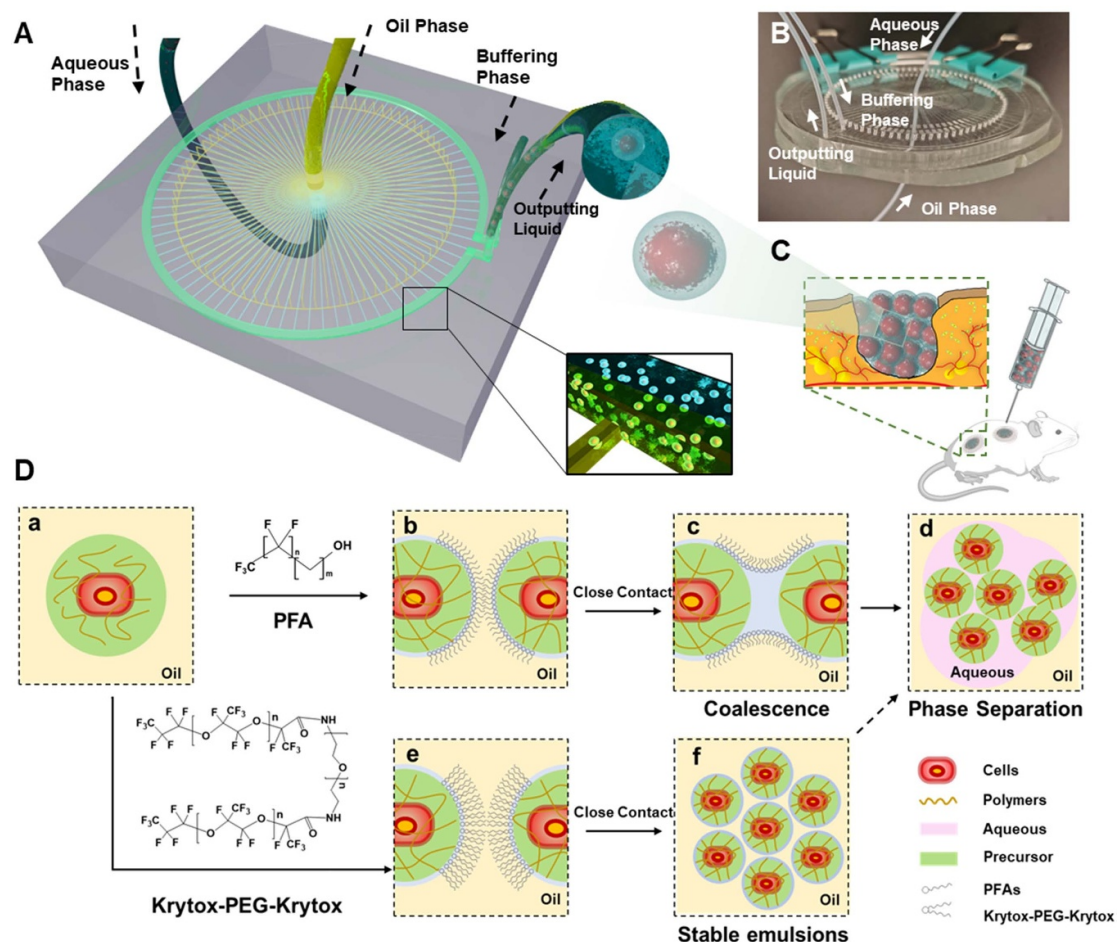
Figure 1. Schematic illustration of the one-step microfluidic strategy for large-scale production of cell-laden microgels using metastable emulsion combined with microfluidic integration into one chip. (A) The multi-layered structure of the 80× DMUs integrated chip. (B) Photograph showing the 80× DMUs in the integrated microfluidic chip connected by inlet and outlet tubes. (C) Schematic diagram showing the use of microfluidic-generated stem cell-laden microgels for the treatment of diabetic rat's skin wound. (D) The mechanism of the formation of cell-laden alginate microgels based on the metastable emulsion using short-chain amphiphilic PFAs as the pseudo-surfactant, in comparison to the conventional multiple-step method based on stable emulsion using stable surfactants such as Krytox-PEG-Krytox. Specifically, hydrogel precursor solution mixed with cells is emulsified using fluorinated oil HFE 7100 containing either amphiphilic short-chain PFA or Krytox-PEG-Krytox as the surfactant. (a) Droplets can be formed using different surfactants, which are further triggered to gel immediately. For metastable emulsions prepared by using PFA as pseudo-surfactant (a, b), the aqueous droplets completely solidified cell-laden microgels that eventually coalesce upon close contact, thereby inducing the phase-separation between oil and water phase ((b), (c)). Direct extraction of the encapsulated cells from the emulsion into the aqueous phase containing cell culture media (d). In contrast, for stable emulsions prepared by a tri-block surfactant, droplets remain stable without showing coalescence ((e), (f)). Such a system requests extra time- and labor-consuming steps to break the emulsion and transfer cells into culture media.

and a perfluoroalkane chain which can maintain the water/oil interface but do not produce stable emulsions due to the limited steric hindrance provided by the small hydrophobic size [43]. We hereby hypothesize that amphipathic PFAs can function as surfactants to enable droplet formation and temporarily maintain their stability before coalescence upon close contact (figure 1(D)). By triggering the gelation of the droplets containing hydrogel precursors before droplet coalescence, we can integrate emulsification, in-drop gelation and de-emulsification into a one-step process (figure S1 (available online at stacks.iop.org/BF/14/035015/mmedia)). Here, a previously reported in-drop triggering-crosslinked alginate system with a very rapid gelation process is adopted [10, 36, 39]. Specifically, the dispersed phase

is composed of alginate precursor solution containing bioactive cargoes and ethylenediaminetetraacetic acid conjugated calcium (Ca-EDTA), while the continuous phase contains fluorocarbon oil (HFE7100, 3M) with 5 v/v % PFA surfactant and 0.1 v/v% acetic acid as the crosslinking initiator. Upon droplet formation, the diffusion of acetic acid from the oil phase into the aqueous drops lowers the pH and subsequently triggers the release of Ca^{2+} ions, thus resulting in the gelation of alginate microgels. The Ca-alginate gelation process can be completed within 50 s [36], which allows microgel solidification before droplet coalescence. Moreover, since alginate precursor is of high viscosity, this makes it difficult to produce small droplets using traditional flow-focusing microfluidic devices; therefore, alginate can

be a representative model material to demonstrate the efficacy and versatility of our microfluidic technique for microgel fabrication. Beside the favorable handling properties, the advantageous biological functions of alginate such as biocompatibility, low immunogenicity, high permeability, and ease of chemical functionalization can further ensure the viability and functionality of the encapsulated cells, and offer high degree of control on engineering the biophysical and biochemical extracellular environmental cues, thereby serving as a powerful platform for cell niche-remodeling and regenerative medicine [5, 44]. This metastable droplet-templating strategy combining with the rapid-crosslinking alginate system enables the continuous generation of microgels, which is critical for the scale-up production of cell-laden microgels.

2.2. PFAs as pseudo-surfactant for the formation of metastable emulsion

We perform an in-depth investigation of the metastable emulsion system and optimize the fabrication parameters for the continuous generation of monodisperse microgels. Three representative amphiphilic PFAs with different numbers of fluorocarbon chains (N_{FC}), i.e. 2,2,3,3,4,4,4-Heptafluoro-1-butanol (PFB, N_{FC} = 3), 1H,1H,2H,2H-perfluoro-1-octanol (PFO, N_{FC} = 5), and 1H,1H,2H,2H-perfluoro-1-decanol (PFD, N_{FC} = 7) (figure S2(A), supporting information), are selected to study their capability of stabilizing the emulsion. The efficiency of the surfactants can be evaluated by the change of the water/oil interfacial tension, γ, as a function of the surfactant's concentration. Without using any surfactants, the interfacial tension γ between de-ionized water and fluorinated oil (HFE7100, 3M) is 50.3 $\pm$ 0.6 mN m^{-1}. The decrease of γ value reaches a plateau as the surfactant concentration decreases to the threshold concentration, which is known as critical micelle concentration (CMC) (figure 2(A)). Hence, increasing PFA concentrations would lead to a relatively linear decline in γ values below the CMCs, which are in the range of 2–5 v/v%. Above the CMCs, the decline of γ values slows down as the surfactant concentration increases. Besides, the efficacy of PFAs reducing the interfacial tension decreases with the decrease of N_{FC} of PFA molecules, evidenced by the significantly reduced interfacial tension using PFAs with longer fluorocarbon chains (figure 2(A)). These findings suggest that PFAs can be well organized at the water/oil interface, thereby reducing the interfacial tension and further facilitating the generation of monodisperse emulsion droplets [19].

To demonstrate the feasibility of using PFAs for the droplet generation, we use a cross-junction dropmaker with a straight downstream channel to monitor the behavior of droplets (figure 2(B) and S3, supporting information). The droplets are stable using PFAs as the surfactant (figure 2(C(i))). However, the

collision of drops can be observed in the gradually widening collection channels, thereafter, inducing the coalescence of these droplets due to the poor capability of PFAs to stabilize the emulsion (figure 2(C(iii-a))). In contrast, droplet coalescence is not observed in the straight collection channel where the droplets do not touch one another (figure 2(C(iii-b))). In addition, the concentration of PFA surfactants also affects the droplet coalescence upon close contact, evidenced by the prolonged coalescence process of two closely contacted droplets upon using PFA with a high concentration (figure S2(B), supporting information). This suggests that we can fine-tune the stability and coalescence of droplets by tailoring the structure of the downstream channel and the concentration of PFA surfactants.

To investigate the effect of fluorocarbon chain length on microgel size, we prepare alginate microgels with different PFAs, and find PFAs with shorter fluorocarbon chains narrow down the size distribution of the alginate microgels at the same concentration (e.g. CV = 2.4% for PFB, CV = 2.7% for PFO) (figure 2(D)). Moreover, different PFAs display various degrees of cytotoxicity reflected by the significantly low cell viability of fibroblasts cultured in PFB-saturated cell culture media compared to PFO and PFD-saturated ones. Additionally, the viability of cells encapsulated in alginate microgels prepared using PFB shows significantly lower viability of 50.37 $\pm$ 1.16% than that of PFO (96.97 $\pm$ 0.57%), PFD (95.33 $\pm$ 1.01%) and the control group (98.57 $\pm$ 0.91%) (figure 2(E)). This is presumably due to the increased solubility of PFB with shorter fluorocarbon chains in water thereby enhancing the cytotoxicity (figure S4, supporting information). Considering the capacity of emulsification, low cytotoxicity and easy preparation, PFO is selected for the further study. We further investigate the effect of flow rate ratio Q_{oil}/Q_{aqu} and surfactant concentration on the droplet formation, where Q_{aqu} is the flow rate of the aqueous phase and Q_{oil} is the flow rate of the oil phase. Three different flow patterns can be observed by tuning Q_{aqu} and Q_{oil}, including squeezing, dripping and jetting as shown in figure 2(F). Specifically, the flow rate ratio Q_{oil}/Q_{aqu} ranging from 5 to 80 results in the dripping regime, which is a preferable condition for the formation of monodisperse droplets [45]. Increasing PFO concentration and reducing Q_{oil}/Q_{aqu} values lead to the dripping regime. Specifically, at a fixed Q_{oil}/Q_{aqu} ratio, increasing PFO concentration effectively narrows the size distribution of microgels, but the influence on the average size of microgels is negligible, which can be attributed to the reduced interfacial tension (figure 2(G)). Moreover, increasing flow rate ratio Q_{oil}/Q_{aqu} decreases the average particle size but enlarges the size distribution (figure 2(H)). To summarize, these results suggest that PFAs can function as pseudo-surfactants for the formation of metastable emulsion droplets, which act
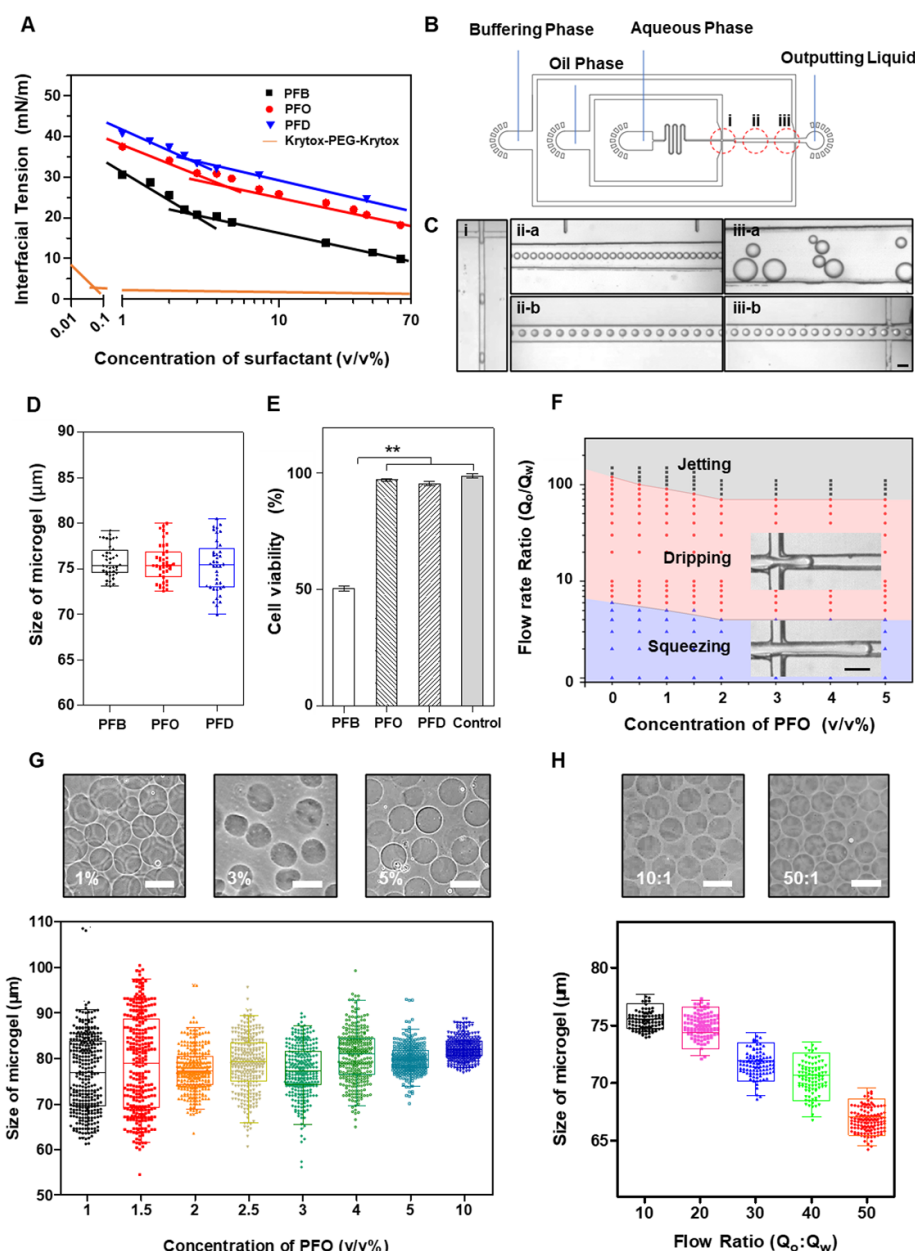
Figure 2. Demonstration of using PFAs as pseudo-surfactant for the formation of metastable emulsion droplets and the continuous generation of alginate microgels. (A) The effect of surfactant concentrations on the interfacial tension between water and fluorinated oil (HFE 7100). Previously reported stable tri-block Krytox-PEG-Krytox surfactant is compared with 2,2,3,3,4,4,4-Heptafluoro-1-butanol (PFB), 1H,1H,2H,2H-perfluoro-1-octanol (PFO) and 1H,1H,2H,2H-Perfluoro-1-decanol (PFD) as pseudo-surfactants. (B) AutoCAD design of the single-DMU microfluidic chip for droplet formation and the investigation of droplet behavior in the downstream channel. A classical flow-focusing channel is used for droplet formation, followed by a straight downstream channel in which droplets may collide. Another flow-focusing channel is designed to introduce the buffering phase. (C) Light microscopic images showing the behavior of droplets at different locations in the microfluidic chips (i)–(iii). The width of the downstream channel increases from 50 μm to 500 μm. This leads to the collision and coalescence of the droplets due to the increased flow resistance and the absence of surfactant (ii-a) and (iii-a). In comparison, in the straight channel (width of 100 μm) droplets do not collide due to the negligible change in flow resistance (ii-b) and (iii-b). The oil to water flow rate ratio Q_{oil}/Q_{aqu} is set to 10, with a flow rate of aqueous phase $Q_{aqu} = 100\,\mu l\,h^{-1}$. Scale bars are 100 μm. (D) Box chart showing the size distribution of the resulting alginate microgels produced using different PFAs as surfactants under the same fabrication parameters. As the length of the fluorocarbon chain increases in the PFA molecules, the distribution of microgel size become wider. (E) The viability of encapsulated rat MSCs using different PFAs as surfactants (5 v/v % PFA in HFE 7100) under the same fabrication parameters. Cells cultured on tissue culture plates are set as control. $**P < 0.01$. (F) Phase diagram showing flow conditions for stable formation of droplets using PFO as the surfactant. Square, circle, and triangle denote jetting, dripping, and squeezing, respectively. Inserted microscope images showing flow patterns generate in the microfluidic device at different preparation parameters. (G) The size distribution of the resulting alginate microgels as a function of PFO concentrations ($Q_{oil}/Q_{aqu} = 10$, $Q_{aqu} = 0.1$ ml h^{-1}). The size distribution of microgels narrows with increasing PFO concentration. Scale bars are 100 μm. (H) The size distribution of the resulting microgels as a function of flow rate ratios (Q_{oil}/Q_{aqu}) (5 v/v % PFO, $Q_{aqu} = 0.1$ ml h^{-1}). The increase of Q_{oil}/Q_{aqu} results in a decrease in the size of microgels. Scale bars are 100 μm.

as the template for generating microgels in a controllable and continuous manner.

2.3. Optimization of integrated chip design based on computational simulation

We further design integrated device containing multiple parallelized DMUs that adapts to the metastable emulsion system and allows the scale-up production of cell-laden microgels. We develop multiple-layered integrated polydimethylsiloxane (PDMS) device and further optimize the microchannel's dimension by computational simulation. Specifically, two design criteria should be considered, (a) all fluids should be apportioned equally among DMUs to achieve a rather narrow size distribution of the droplets; (b) the flow rate of both input and output liquids should be relatively high to avoid cargo aggregation or sedimentation that can block the device.

Regarding the design of input channels, previously reported integrated chips typically consist of channels parallelized horizontally [22, 46] or radially [24, 33]. The horizontal parallelization can easily increase the number of DMUs; however, fluid distributions may suffer from large variation between neighboring channels [46]. Here, we design a radially parallelized device to ensure all liquids are apportioned equally, avoiding the decay of flow rate between each DMU (figure 3(A)). As microgels are massively produced in the device, rapid removal of the microgels out of the channel is critical as they are sticky and likely to adhere to the chip, thus blocking the channel. Therefore, we design a toroidal collection channel, allowing all liquids to flow unidirectionally and converge into one collection channel (figure S5, supporting information). By further introducing an extra aqueous phase at a high flow rate in the toroidal collection channel, we can neutralize the acid used for triggered-gelation of alginate, and avoid channel blockage caused by the further crosslinking reaction between microgels.

To optimize the channel design, we simulate the fluid behavior in the microfluidic chip using CFD simulation. The prerequisites for the simulation include: (a) the fluid resistance distribution in 3D structure of the microchannels is simplified by a 2D circuit diagram (figures 3(B) and (C)), in which the hydraulic resistance R of each DMU is denoted as R_u and the resistance of toroidal collection channels between DMUs as R_c [33, 44]. (b) The hydraulic pressure at the outlet of the collection channel has the minimal value, p_{min}, and the inlet of oil phase has the maximal hydraulic pressure p_{max}. To simplify the calculation, we set $p_{min} = 0$, and $p_{max} = 1$. Thus, the values of local fluid resistance $h = QR$ (Q is the local flow rate) within the chip can be identical to the local hydraulic pressure difference Δp. (c) To ensure a narrow size distribution of the resulting droplets, the simulation aims to facilitate the identical distribution of flow rates in each DMU. This requires the hydraulic

resistance of the collection channels from one DMU to its neighbor (R_c) to be negligible compared to the resistance of each DMU (R_u), i.e. $R_c \ll R_u$ [46]. Specifically, this requires the sum of fluid resistance h_{ci} in the collection channels down stream of each DMU should be significantly lower than the fluid resistance h_u of each DMUs, i.e. $Sum(h_{ci})/h_u < 1\%$ (supporting information and figure S6) [22, 33].

We obtain the heat maps of hydraulic pressure p and flow velocity of the chip; thus, we can obtain the values of fluid resistance h of each location. The heat map shows the obvious difference in fluid resistance between DMUs h_u, evidenced by the difference between No. 1 and No. 16 DMU in the heat map (figures 3(D)–(F)). In addition, the decline of fluid resistance along the flow direction is noticeable, but the ratio of $Sum(h_{ci})/h_u$ is still higher than 3% (figure 3(L)). Such large difference of fluid resistance in the toroidal channel further results in an inhomogeneous distribution of flow velocity between DMUs (figure 3(G)), in which up to 4.6% difference in flow velocity at the outlet of each DMU can be observed (figure 3(M)). These differences in fluid resistance and flow velocity can lead to wide size distribution of the resulting droplets/microparticles [19].

To address this issue, we increase the fluid resistance h_u by adding a serpentine channel along each DMU, so that local variance in fluid resistance and flow velocity between DMUs can be reduced (figures 3(H) and (K)). This design efficiently reduces the difference in the distribution of fluid resistance between DMUs (figures 3(H)–(J)), decreases the ratio of $Sum(h_{ci})/h_u$ to less than 1% (figure 3(L)), and minimizes the flow velocity difference between DMUs (figures 3(K) and (M)). Furthermore, this design strategy is also effective for an 80× DMUs integrated chip, evidenced by the simulation results (figure S7, supporting information). Generally, our result from computational simulation provides a cost-efficient tool for the design and optimization of integrated chips for the large-scale production of monodisperse droplets.

2.4. Experimental demonstration of the large-scale generation of microgels

We further evaluate the performance of the optimized chip containing 16× DMUs for cell encapsulation using alginate microgels (figures S8 and S9, supporting information). Based on the input directions of oil and aqueous phases, droplets can be produced through either T-junction or flow-focusing mode (figure S9(C), video S2, supporting information), thereafter, triggering on-chip gelation is completed before converging into the toroidal channel (figure 4A(a, b), video S3, S4, supporting information). We first test the preparation parameters of the integrated chip based on a stable emulsion system using Krytox-PEG-Krytox [10] as the surfactant (figure 4A(a)). Droplets with a narrower
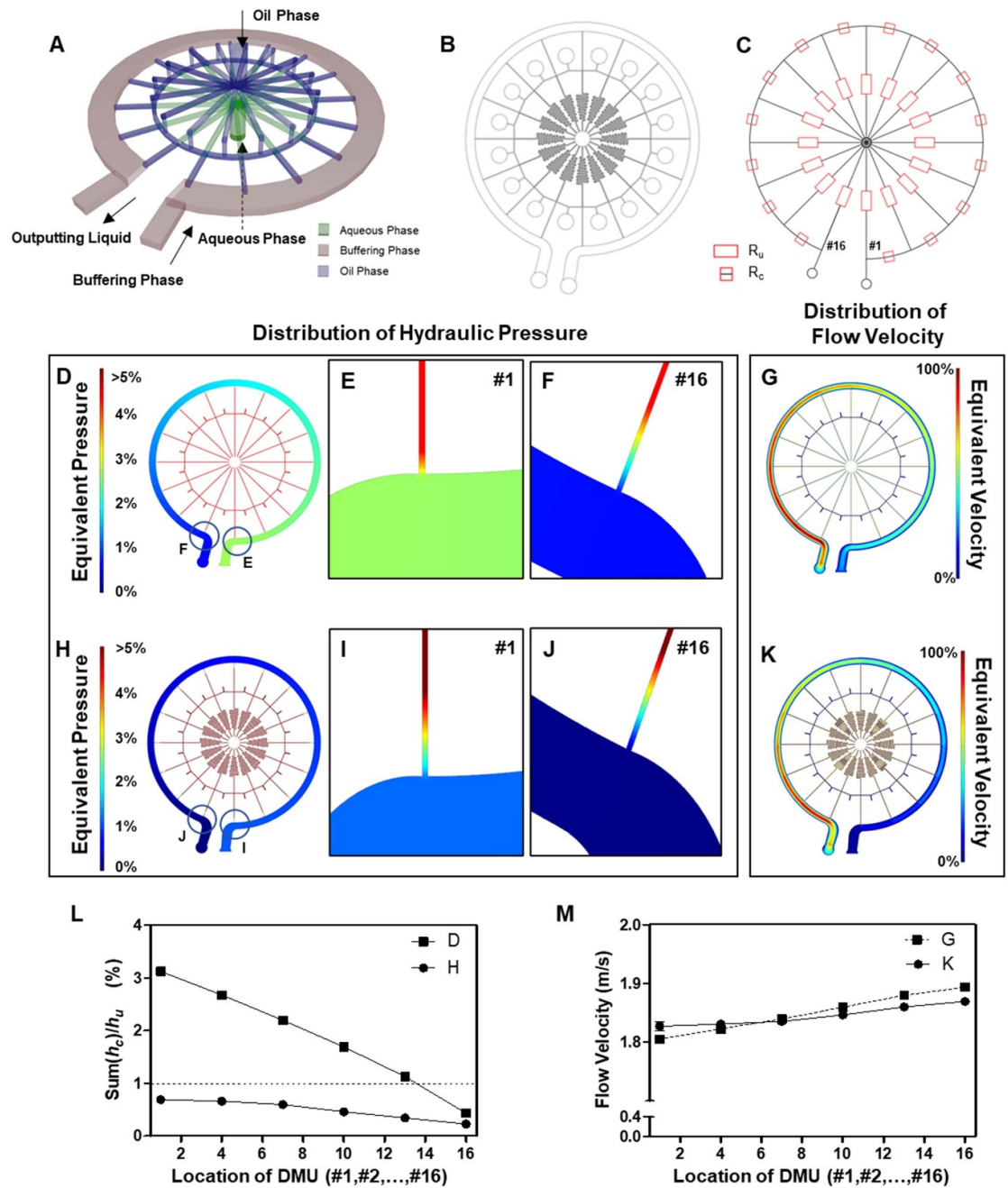
Figure 3. The design of integrated microfluidic chip and optimization of channel geometry based on computational fluid simulation by COMSOL Multiphysics. (A) 3D structure of the integrated microfluidic chip containing 16 circularly parallelized cross-junctions in generation layer, and the corresponding AutoCAD design is shown in figure (B). (C) Simplified 2D circuit diagram for hydraulic resistances within the integrated chip design. The distribution of hydraulic resistance in the integrated chip is simplified using a circuit diagram from generation layer design, in which the DMUs are connected in parallel, and the output liquid from each DMU is collected in series. The circularly parallelized elements represent the hydraulic resistance of DMUs R_u; the annular elements represent the fluid resistance of the collection channel R_c per segment. (D) Heat map, showing the distribution of hydraulic pressure throughout the chip. The minimal hydraulic pressure located at the outlet of the collection channel is set to zero so that the local hydraulic pressure at every point in the chip can be presented by a percentage value after being normalized to the maximum pressure. (E) and (F) Heat maps at higher magnification showing the distribution of hydraulic pressure at the cross-junction between DMU and the collection channel. Apparently, the first DMU (E) shows larger differences in local hydraulic pressure than that of the last DMU (F), suggesting inhomogeneity in fluid dynamics between DMUs in such chip design. (G) Heat map, showing the distribution of flow velocity throughout the chip. (H)–(J) Heat maps of low (H) and high magnification (I) and (J) showing the distribution of hydraulic pressure in the chip with resistance-control structures. (K) Heat map, showing the distribution of flow velocity in the chip with resistance-control structures. (L) Quantification of local fluid resistance Sum(h_{ci}) of collection channel downstream of each DMU in proportion to the fluid resistance of DMUs h_u based on simulation results of hydraulic pressure (D), (H). The effect of adding a resistance-control structure is reflected by the change in the distribution of fluid resistance. (M) Quantification of flow velocity at the cross-junction between DMUs and the collection channel based on simulation results of flow velocity (G), (K).
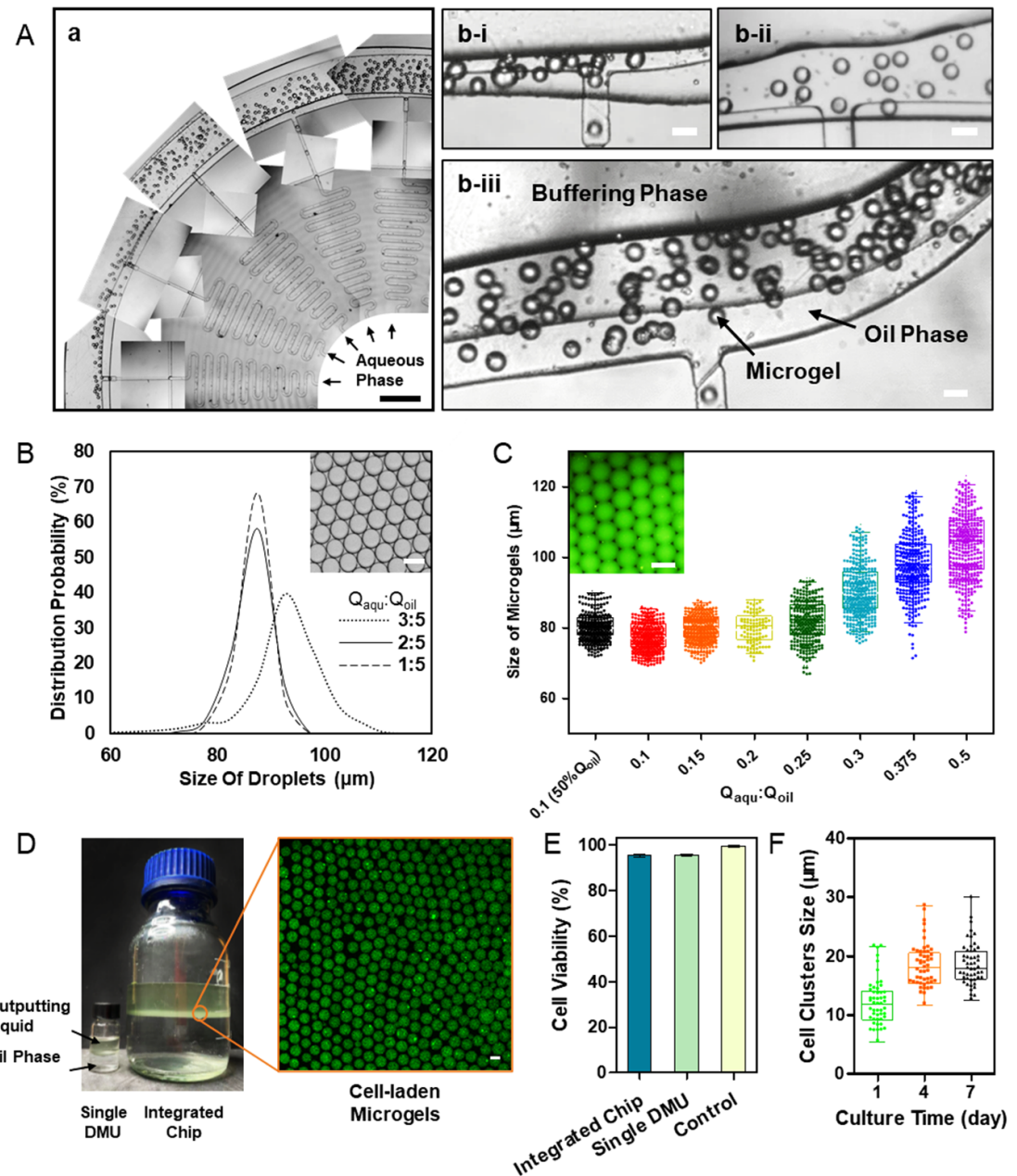
Figure 4. Experimental data of the integrated chip for large-scale production of alginate microgels. (A) Bright field of microscopic images showing the flow dynamics at different locations of the integrated chip. (a) Stacked images showing the production of cell-laden microgels using 16× DMUs integrated chip. Scale bar is 1000 μm. (b) Images showing the flow states at outlets of the No. 1 (b-i), 8 (b-ii), and 16 DMUs (b-iii) of the integrated chip for microgels production. Scale bar is 100 μm. (B) The size distribution of the resulting droplets produced with different flow rate ratios Q_{aqu}/Q_{oil} at a fixed Q_{oil} (16 ml h^{-1}). Inserted microscopic image showing the droplets produced by 16× DMUs integrated chip in a flow ratio of Q_{aqu}/Q_{oil} = 1:5 and Q_{oil} = 16 ml h^{-1}. Scale bar is 100 μm. (C) The size distribution of the resulting microgels produced with different flow rate ratios Q_{aqu}/Q_{oil} at a fixed Q_{oil} (24 ml h^{-1}). Inserted fluorescent microscopic image showing fluorescein-labeled alginate microgels produced by 16× DMUs integrated chip (CV = 3.60%) at the flow ratio of Q_{aqu}/Q_{oil} = 1:5 and Q_{oil} = 16 ml h^{-1}. Scale bar is 100 μm. (D) Photograph showing the output liquids collected from 80× DMUs integrated chip versus single-DMU for 1 h fabrication. Fluorinated oil is heavier than the aqueous phase dispersed with cell-laden microgels (labeled with fluorescein) located at the lower part of the aqueous phase. Cells are transfected by green fluorescent protein. Scale bar is 100 μm. (E) The viability of encapsulated rat MSCs using a single-DMU versus 16× DMUs integrated chip. Cells cultured on cell culture plates are used as control. (F) The diameter distribution of cell clusters formed in the alginate microgels at different time points of *in vitro* culture.

size distribution can be obtained with a relatively low flow rate ratio evidenced by the CV values lower than 4% for Q_{aqu}/Q_{oil} < 1:2.5, but a higher flow rate ratio Q_{aqu}/Q_{oil} causes a wide size distribution (CV = 8.36% for Q_{aqu}/Q_{oil} = 1:1.67, figure 4(B)). In contrast, a narrower size distribution

(CV < 4%) of microgel can be obtained at a flow rate ratio Q_{aqu}/Q_{oil} < 1:4 (figure 4(C)) by our meta-stable droplet-templating strategy using PFO as the pseudo-surfactant. Moreover, we also generate cell-laden alginate microgels using integrated chip with 80 cross-junctions (figure 1(B)). Considering the

limited flow rate of aqueous phase to avoid high shear force on the encapsulated cells, we maintain $Q_{aqu} \leqslant 100 \ \mu l \ h^{-1}$ for each DMU in the integrated chip. This allows the generation of alginate microgels (CV = 7.17%) at a production rate of $10 \ ml \ h^{-1}$ (figures 4(D) and S10, video S5, supporting information).

We further use this microfluidic system for MSC encapsulation (video S6, supporting information). The integrated chip shows a similar degree of control on the microgel size and encapsulation efficiency of the resulting cell-laden microgels compared to the single-DMU device, by tailoring the dimension of the microchannel and the concentration of the cell suspension. For instance, at a concentration of 2×10^6 cells ml^{-1}, we obtain 57.2% of empty microgels, 24.6% of single cell-laden microgels and 18.2% of multiple cell-laded microgels, which is similar to that of the single-DMU chip at the same cell concentration (figure S11, supporting information). The experimental data depicts an excellent correlation of cell distribution to the theoretical values of Poisson distribution for cell concentrations at 2×10^6 cells ml^{-1}. The encapsulation of primary rat MSCs in alginate microgels using the integrated chip exhibits high viability of >95%, similar to that of the single-DMU chip (figure 4(E)). By further using alginate conjugated with cell attachment motif (arginine-glycine-aspartic acid, RGD) as artificial ECM [10], we observe continuous proliferation of encapsulated cells in alginate microgels during *in vitro* culture (figure S12, supporting information). The encapsulated cells maintain a relatively spherical shape in RGD-alginate matrix, most likely due to the crosslinking network of alginate that restricts cell movement and spreading [10, 11, 28]. Syto 9 nuclei staining reveals that the majority of cell-laden microgels initially contain single cells after encapsulation, and they gradually proliferate after a couple of days of *in vitro* culture while still maintaining a spherical shape (figure S12, supporting information). In addition, we observe continuous growth of the average size of MSC clusters, increasing from $12.1 \pm 1.9 \ \mu m$ to $18.6 \pm 1.8 \ \mu m$ after seven days (figure 4(F)).

2.5. Single rMSC-laden microgels as injectable fillers for the treatment of skin wound

We use a diabetic-rat full-thickness skin wound model [47] to demonstrate the feasibility of using the single MSC-laden alginate microgels produced by our scale-up method as injectable fillers for tissue regeneration (figure S13, supporting information) [5, 48]. At day 7 post-implantation, the wounds close about $40.89 \pm 4.10\%$ and $46.52 \pm 3.63\%$ after being filled with MSC-laden alginate microgels and naked MSCs mixing with alginate microgels, respectively, whereas only $17.29 \pm 5.18\%$ wound closure for bare microgels treatment and $29.86 \pm 5.02\%$ for the control group (figures 5(A) and (B)). This indicates that the

local introduction of MSCs can accelerate wound healing. We perform histological hematoxylin-eosin (H&E) stainings to investigate the regenerative capacity of different treatments (figure 5(C)). The result of the epithelia gap measurement displays similar trend to the wound closure (figure 5(D)). Further quantification of the thickness of the granular tissues confirms the quality of wound healing, where thick newly formed granular tissues suggest better skin regeneration; however, granular tissues thicker than the baseline of the original skins imply hyperproliferation of granulation tissues which might hamper the normal physiological wound healing procedure. We observe that MSC-laden microgel group generates more granular tissues ($763.7 \pm 56.4 \ \mu m$ in thickness) than the cell mixing with microgel group ($340.6 \pm 61.2 \ \mu m$) and the control group ($435.1 \pm 35.1 \ \mu m$) (figure 5(E)). Noticeably, wounds treated with only microgels show more newly formed granular tissues even overgrowing the original skin ($1104.3 \pm 51.7 \ \mu m$). This implies that the introduction of alginate microgels might lead to a hyperproliferation of granulation tissue, which can hamper the normal physiological wound healing procedure. Further histoimmunofluorescent stainings reveal different immune responses for each group. A substantially higher amount of CD3-positive T cells is observed at the wounds treated with naked MSCs with microgel compared to the other groups (figures 6(A)–(C)), and the same tendency also occurred on inducible nitric oxide synthase (INOS)-positive macrophages of these groups (figures 6(D) and (E)). These are most likely due to the strong immunogenicity provoked by the exposed allogenic MSCs. In contrast, the introduction of MSC-laden microgels shows much less presentation of both T cells, macrophages (F4/80 staining), and show less M1 polarization rate of macrophage (INOS staining), all of which are at the same level to the control group and these can be attributed to the immunomodulatory capability of the encapsulated allogenic MSCs and the shielding effect provided by the hydrogel coatings against the host immunoclearance [49, 50]. Overall, these results indicate that MSC-laden microgels possess the capacity to promote wound healing process through immunoregulation.

To generate cell-laden microgels in large-scale is one of the most challenging techniques for droplet-templating microfluidics since cells are vulnerable to shear force, hypoxia and cytotoxic chemicals, which makes it impossible to adapt to currently available scale-up techniques. Here, we propose an innovative metastable droplet-templating method to allow one-step, continuous generation of cell-laden alginate microgels using a conventional flow-focusing microfluidic design. The use of PFAs as pseudo-surfactant to form metastable droplets can efficiently template microgel formation and on-demand demulsification. Besides, unlike conventional surfactants for cell encapsulation that are expensive and
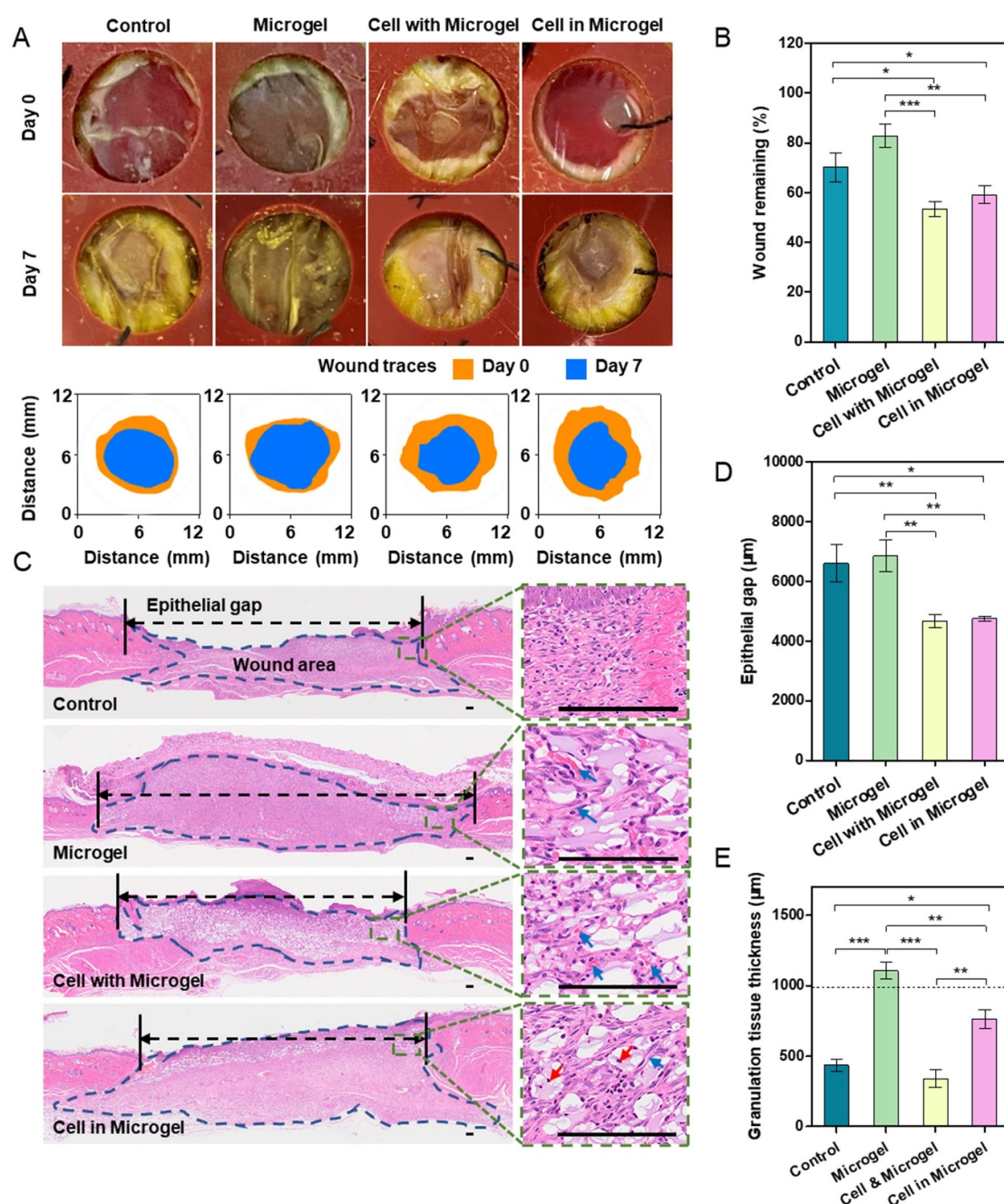
Figure 5. Skin-wound healing capacity of MSCs encapsulated in alginate microgels. (A) Representative images of wound closure and the trace of wound-bed closure after seven days of treatment. (B) Schematic diagram showing the wound closure of diabetic rat. After one week, wounds treated by cell-laden microgels and cell/microgel mixture show significantly faster wound healing than the untreated negative control and bare microgel-treated group ($N = 6$). (C) H&E staining of tissue sections indicate wound closure and the growth of granulation tissue after different treatments for one week. Blood capillaries infiltrating around the microgels are marked by blue arrows, and MSCs retained in microgels are marked by red arrows. Scale bar is 500 μm in $4\times$ images and 20 μm in $63\times$ images, respectively. (D) Quantification of the epithelial gap and (E) the thickness of granulation tissue from H&E staining of tissue sections. $^*P < 0.05$; $^{**}P < 0.01$; $^{***}P < 0.005$.

difficult to synthesize, using PFAs as surfactants can substantially reduce the cost, by more than 90%. Furthermore, to address the problems such as poor control over particle size distribution and channel blockage upon microfluidic scale-up [35], we specifically design a class of 3D integrated chips which show the production rate of two orders of magnitude higher than previous microfluidic techniques for cell-laden microgel formation [6, 30]. Moreover, we develop

a method based on computational simulation to predict fluid distribution in microchannels and to optimize complicated chip design in a cost-efficient way. Taken together, this design rationale for large-scale microgel production can be expanded to a wider range of hydrogel materials, and can strongly contribute to the emerging biomedical applications like 3D bioprinting, modular tissue engineering and cell-based therapies.
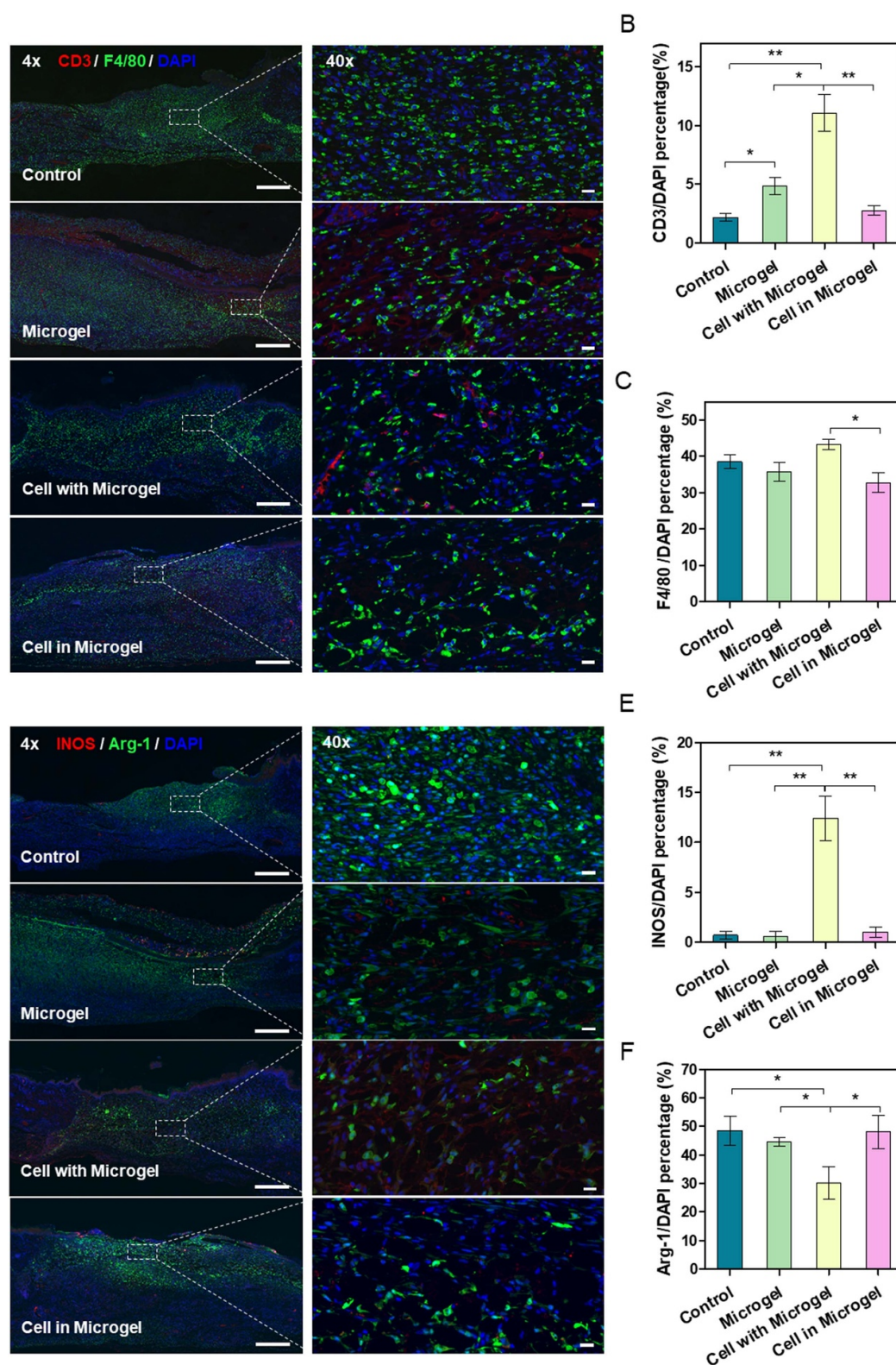
Figure 6. Inflammatory responses and macrophage phenotypes of the skin wound under different treatment closure after seven days. (A) Representative histoimmunofluorescent images of CD3-positive (T cells: red) and F4/80-positive (macrophage: green) in the wound after different treatments. Quantitative analysis of specific CD3-positive (B) and F4/80-positive (C) number to the number of DAPI (nuclei: blue). (D) Representative histoimmunofluorescent images of INOS-positive (M1 macrophage: red) and Arg-1-positive (M2 macrophage: green) in the wound after different treatments. Quantitative analysis of specific INOS -positive (E) and Arg-1-positive (F) number to the number of DAPI (nuclei: blue). Scale bars are 500 μm in 4$\times$ images and 20 μm in 40$\times$ images. $^*P < 0.05$; $^{**}P < 0.01$.

3. Conclusion

In summary, we develop a novel microfluidic strategy for the scale-up generation of single-cell laden microgels based on metastable droplet-templating and microfluidic integration. We demonstrate the generation of single cell-laden microgels at a production rate larger than 10 ml h^{-1} cell suspension while maintaining the monodispersity and cell viability, which is substantially higher than previously reported techniques. This microfluidic strategy represents a significant step forward in high-throughput cell microencapsulation technology, and can offer a new route for clinically relevant applications of cell-laden microgels in tissue engineering, 3D bioprinting and cell therapies.

4. Experimental section

4.1. Material

1H,1H,2H,2H-perfluoro-1-octanol (PFO), 2,2,3,3, 4,4,4-Heptafluoro-1-butanol (PFB), 1H,1H,2H,2H-Perfluoro-1-decanol (PFD), dimethyl sulfoxide, arginine-glycine-aspartic acid (Arg-Gly-Asp, RGD), sodium alginate, 4-(2-hydroxyethyl)piperazine-1-ethanesulfonic (HEPES) acid, ascorbic acid, streptozotocin (STZ), paraformaldehyde, dexamethasone, β-glycerophosphate, alizarin red and paraformaldehyde are purchased from Sigma-Aldrich (USA). Dulbecco's modified Eagle's medium (DMEM), minimal essential medium α (αMEM), fetal bovine serum (FBS), penicillin/streptomycin are purchased from Gibco (USA). Disodium-EDTA, lysis buffer, 1-ethyl-(dimethylaminopropyl) carbodiimide, N-hydroxy-sulfosuccinimide are purchased from Solarbio (China). Fluorocarbon oil (Novec 7100 Engineered Fluid) is purchased from 3M (USA). PDMS (RTV-615) is purchased from Momentive (USA). Calcium chloride, ethylenediaminetetraacetic acid disodium salt (Na$_2$EDTA), sodium hydroxide, acetic acid and all the other chemicals are purchased from DAMAO (China).

4.2. Measurement of interfacial tension via pendant drop

We measure the interfacial tension between the aqueous phase and the oil phase under different concentrations of PFAs by the contact angle meter (CA100A, Innuo, China). Measurements are performed by using a syringe pump and camera on the contact angle meter. The oil phase containing surfactants is extruded from a flat-tipped needle with an outer diameter of 0.70 mm into the cuvette with deionized water and the process is photographed before the droplet falls from the needle. The interfacial tensions are further analyzed using the software in the instrument.

4.3. Evaluation of droplet stability upon using PFAs as the surfactant

Microfluidic devices made of PDMS are fabricated by the soft lithography protocol [38], which is described in the supplementary information. For the continuous generation of droplets, deionized water is used as the aqueous phase, and fluorocarbon oil (HFE7100, 3 M, USA) consisting 5 v/v % PFA (PFB, PFO, or PFD) is used as the oil phase. All syringes are connected to the inlet of the PDMS devices via polyethylene tubes with an inner diameter of 0.38 mm (Smiths Medica, UK). The flow rates are individually controlled by different syringe pumps (lsp-1b, Longer, China). We kept the flow rate of the aqueous phase Q_{aqu} constant at 100 μl h^{-1} and the flow rate of oil phase Q_{oil} at 1000 μl h^{-1}. To determine the stability of droplets formed with different concentrations of PFAs, we use a high-speed camera (ispeed.221, iX Cameras, UK) and an optical microscope (ae2000, Motic, China) to observe the merging behavior of droplets in a single-DMU device.

4.4. Microfluidic generation of alginate microgels using metastable emulsion by the single-DMU device

For microfluidic generation of alginate microgels, a solution containing 1 w v^{-1} % Na-alginate and 50 mM Calcium-EDTA as a crosslinker [6, 10] is used as the aqueous phase, and fluorinated oil HFE7100 consisting 0.1 v/v % acetic acid and surfactant is used as the oil phase. 5 v/v % PFA (PFB, PFO or PFD) or 1 v/v % Krytox-PEG-Krytox is used as the surfactant to compare their effects on the formation of microgels. Another aqueous solution containing 25 mM HEPES (pH = 7) is used as the buffering phase to neutralize the acid and facilitate the coalescence of the droplets containing Ca-alginate microgels. All syringes are connected to the PDMS devices via polyethylene tubes with an inner diameter of 0.38 mm. The flow rates of aqueous Q_{aqu}, oil Q_{oil} and buffering phases Q_{buffer} are individually controlled by different syringe pumps (lsp-1b, Longer, China). Q_{aqu} is kept constantly at 100 μl h^{-1}, and Q_{oil} and Q_{buffer} are both kept at 1000 μl h^{-1}. The high-speed camera and optical microscope are used to monitor the formation and separation of microgels.

4.5. CFD simulations

Commercially available software (COMSOL Multiphysics, COMSOL Co.) is used to simulate fluid dynamics in the microfluidic channels of different geometries (designed by Auto CAD, Autodesk Inc.). The simulation is performed based on the following prerequisites: (a) The 3D structure of the microchannels is simplified by a 2D circuit diagram (figure 3(C). (b)) The minimal hydraulic pressure located at the outlet of the collection channel is set to zero, so that the hydraulic pressure values throughout the chip can

be normalized by the maximal pressure located at the inlet of the aqueous phase. Thus, the values of local fluid resistance can be identical to that of fluid resistance which can be predicted by simulation. The flow rates of different liquids are used as input information for the simulation. As such, we can obtain the heat maps of the hydraulic pressure (or fluid resistance) and the flow velocity throughout the chip by simulation, in which hydraulic pressure is calculated by flow velocity at each position. The local fluid resistance and flow velocity for each DMU can be further quantified based on the heat maps. All CFD simulations based on the microfluidic chips of different geometries are performed using this setup.

4.6. Fabrication of microgels by integrated chips

For the large-scale generation of alginate microgels by integrated chips containing 16 or 80 cross-junctions, the components of all liquid phases are the same as for the generation by single-DMU devices. For $16\times$ DMUs integrated chips, Q_{oil} for each DMU is kept at 1500 or 750 μl h^{-1} (i.e. total Q_{oil} is 24 or 12 ml h^{-1}), the ratio of Q_{aqu}/Q_{oil} is fine-tuned between 0.1–0.5, and the total Q_{buffer} is kept constant at 24 ml h^{-1}. For $80\times$ DMUs integrated chips, total Q_{aqu} is kept constant at 10 ml h^{-1}, and Q_{oil} and Q_{buffer} are both kept at 40 ml h^{-1}.

4.7. Fabrication of single cell-laden microgels

For cell encapsulation, all devices are sterilized by washing with alcohol followed by UV illumination ($\lambda \sim 254$ nm) for 3 h before use. Synthesis of Arg-Gly-Asp (RGD) conjugated alginate, isolation and culture of rat MSCs are realized according to the previous report [6]. Cells are dispersed in 1 w v^{-1} % alginate solution with a cell density of 2×10^6 cell ml^{-1}, and 50 mM Ca-EDTA. We use HFE7100 containing 5 v/v % PFO and 0.1 v/v % acetic acid as oil phase. About 25 mM HEPES in cell culture medium (DMEM for Hela cells and minimal essential medium α (α-MEM) for rat MSCs, pH = 7.4) is used as the buffering phase to neutralize the acid and retain the encapsulated cells in the aqueous phase. Q_{aqu} for each DMU is kept constant at 100 μl h^{-1} (i.e. total Q_{aqu} is 3.2 ml h^{-1}), Q_{oil} is set at 1000 μl h^{-1}, and Q_{buffer} is constant at 2000 μl h^{-1}. The cell-laden microgels are finally collected using a cell strainer, and then redispersed in cell culture media. The medium is refreshed every three days during *in vitro* cell culture (Hela cells in DMEM and rat MSCs in α-MEM). Cells in the microgels are cultured for seven days. The viability of the encapsulated cells in alginate microgels is measured by a live/dead assay using a LIVE/DEADs® kit (Invitrogen, USA). The cells are stained by Syto 9 nuclei staining (Thermo Fisher, USA). Fluorescent images are captured using a confocal laser scanning microscope (OLYMPUS FV1000, Japan).

4.8. Skin wound healing assessment

The regeneration capacity of skin wound of cell-laden microgels is assessed by using an excisional wound healing model in diabetic SD rats [45, 49]. The animal experiment is carried out in accordance with the regulation of Biomedical and Animal Ethics Committee of Dalian University of Technology and approved with DUT-2021-097. Five to six-week-old male SD rats are used in this study. To build an animal model of diabetes, SD rats are intraperitoneally injected with STZ dissolved in sodium citrate buffer (pH = 4.4) at a dose of 70 mg kg^{-1} of body weight after fasting for 12 h. After one week, the blood glucose levels of rats are measured with a glucose meter (Sinocare, China) after fasting for another 12 h. If blood glucose levels are higher than 16.7 mM, the rats are considered diabetic. Diabetic rats (glucose levels 20.1 ± 1.36 mM) are randomly selected and anesthetized by isoflurane, and the dorsal fur is shaved with depilatory cream (DOVE, Netherland & Canada) and the dorsal skin is then wiped with 75% ethanol. Next, two 8 mm full-thickness wounds are created using a biopsy punch on each side of the dorsum, and both wounds on each mouse are treated similarly. Afterwards, the skin wound cavities are filled with different fillers. Only moved skin tissues is defined as the control group; wound cavity filled with alginate microgels is defined as the microgel group; wound cavity filled with building blocks formed by the mixing of MSCs and microgels is defined as cell with microgel group; wound cavity filled with MSCs-laden microgels is defined as cell in Microgel group (table 1). The wound cavity is eventually sealed using Tegaderm film (3M Inc., USA), and a rubber splint (O.D. $\sim$20 mm; I.D. $\sim$12 mm) is then secured around the wound by a small amount of commercial adhesive (VetBond, 3M Inc., USA) and four interrupted sutures. All animals are housed in controlled conditions for temperature (24 °C) and under a 12:12 h light–dark cycle and fed ad libitum.

At day 0 and day 7, the wound healing process is recorded with a digital camera and the wound area is measured using the image analysis software (Image J). Wound area (%) is calculated as A7/A0 $\times$100%, where A0 is the initial wound area at day 0 and A7 is the wound area at day 7. Afterwards, skin wound tissues are cut down, fixed by 4% paraformaldehyde, and then are embedded followed by being sectioned into slices of 6 μm in thickness. H&E staining is performed to analyze the granulation tissue regeneration and wound closuring.

4.9. Statistical analysis

All data were presented as mean $\pm$ standard deviation. Data were analyzed by GraphPad Prism 5. Statistical differences were analyzed with the one-way analysis of variance and Tukey's post hoc test. $p < 0.05$ was considered as statistically significant.

Table 1. The description of different experimental groups in diabetic rats excisional wound healing model.

Acronyms	Definition	Pre-implantation treatment
Control	Move all skin tissue without any filler materials.	N.A.
Microgel	Skin wound cavity filled with alginate microgels.	Microgels are cultured in growth medium for one day.
Cell with Microgel	Skin wound cavity filled with building blocks formed by the mixing of MSCs and microgels	MSCs are cultured on 2D tissue cultured and mixed with Microgels before injection.
Cell in Microgel	Skin wound cavity filled with MSCs-laden microgels	MSCs are encapsulated in microgels and cultured in growth medium for one day.

Data availability statement

All data that support the findings of this study are included within the article (and any supplementary files).

Acknowledgments

Conflict of interest

The authors declare no conflict of interest.

Author contributions

H Z, L Z, and C A contributed equally to this work; H Z and H W designed the research; H Z, F S, Y G, Y H Z, H L, Y J Z performed research; H Z, Y Z, C R, K S, W H, F C, H N and D A W analyzed data; and H Z, L Z, C A and H W wrote the paper.

ORCID iD

Huanan Wang ⬤ https://orcid.org/0000-0003-3783-1871

References

[1] Jiang W, Li M, Chen Z and Leong K W 2016 Cell-laden Microfluidic Microgels for Tissue Regeneration *Lab Chip* **16** 4482

[2] Lienemann P S, Rossow T, Mao A S, Vallmajo-Martin Q, Ehrbar M and Mooney D J 2017 Single cell-laden protease-sensitive microniches for long-term culture in 3D *Lab Chip* **17** 727–37

[3] Hu Y, Mao A S, Desai R M, Wang H, Weitz D A and Mooney D J 2017 Controlled self-assembly of alginate microgels by rapidly binding molecule pairs *Lab Chip* **17** 2481–90

[4] Ma J, Wang Y and Liu J 2017 Biomaterials meet microfluidics: from synthesis technologies to biological applications *Micromachines* **8** 255

[5] Mao A S *et al* 2019 Programmable microencapsulation for enhanced mesenchymal stem cell persistence and immunomodulation *Proc. Natl Acad. Sci. USA* **116** 15392–7

[6] An C *et al* 2020 Continuous microfluidic encapsulation of single mesenchymal stem cells using alginate microgels as injectable fillers for bone regeneration *Acta Biomater.* **111** 181–96

[7] Dou X Q and Feng C L 2017 Amino acids and peptide-based supramolecular hydrogels for three-dimensional cell culture *Adv. Mater.* **29** 1604062

[8] Hann S D, Niepa T H, Stebe K J and Lee D 2016 One-step generation of cell-encapsulating compartments via polyelectrolyte complexation in an aqueous two phase system *ACS Appl. Mater. Interfaces* **8** 25603–11

[9] Choi C H, Wang H, Lee H, Kim J H, Zhang L, Mao A, Mooney D J and Weitz D A 2016 One-step generation of cell-laden microgels using double emulsion drops with a sacrificial ultra-thin oil shell *Lab Chip* **16** 1549–55

[10] Zhang L *et al* 2018 Microfluidic templated multicompartment microgels for 3D encapsulation and pairing of single cells *Small* **14** 1702955

[11] Chen Q, Utech S, Chen D, Prodanovic R, Lin J M and Weitz D A 2016 Controlled assembly of heterotypic cells in a core-shell scaffold: organ in a droplet *Lab Chip* **16** 1346–9

[12] Panda P, Ali S, Lo E, Chung B G, Hatton T A, Khademhosseini A and Doyle P S 2008 Stop-flow lithography to generate cell-laden microgel particles *Lab Chip* **8** 1056–61

[13] Yeh J, Ling Y, Karp J M, Gantz J, Chandawarkar A, Eng G, Blumling J 3rd, Langer R and Khademhosseini A 2006 Micromolding of shape-controlled, harvestable cell-laden hydrogels *Biomaterials* **27** 5391–8

[14] Li W *et al* 2018 Microfluidic fabrication of microparticles for biomedical applications *Chem. Soc. Rev.* **47** 5646–83

[15] Bong K W, Bong K T, Pregibon D C and Doyle P S 2010 Hydrodynamic Focusing Lithography *Angew. Chem., Int. Ed. Engl.* **49** 87–90

[16] Le Goff G C, Lee J, Gupta A, Hill W A and Doyle P S 2015 High-throughput contact flow lithography *Adv. Sci.* **2** 7

[17] Li H, Wang L, Zhang J, Flynn T, Stephens S and Trinkle C 2017 *Presented at 2017 IEEE 12th Int. Conf. on Nano/Micro Engineered and Molecular Systems (NEMS), A Simple Creation of Freestanding Three-Dimensional Microstructures by Aligned Mask Micromolding for Biomedical Applications (Los Angeles, USA, April 2017)*

[18] Annamalai R T, Hong X, Schott N G, Tiruchinapally G, Levi B and Stegemann J P 2019 Injectable osteogenic microtissues containing mesenchymal stromal cells conformally fill and repair critical-size defects *Biomaterials* **208** 32–44

[19] Zhu P and Wang L 2016 Passive and active droplet generation with microfluidics: a review *Lab Chip* **17** 34–75

[20] de Rutte J M, Koh J and Di Carlo D 2019 Hydrogels: scalable high-throughput production of modular microgels for *in Situ* assembly of microporous tissue scaffolds *Adv. Funct. Mater.* **29** 1900071

[21] Amstad E, Datta S S and Weitz D A 2014 The microfluidic post-array device: high throughput production of single emulsion drops *Lab Chip* **14** 705–9

[22] Jeong H H, Yelleswarapu V R, Yadavali S, Issadore D and Lee D 2015 Kilo-scale droplet generation in

three-dimensional monolithic elastomer device (3D MED) *Lab Chip* **15** 4387–92

[23] Yadavali S, Jeong H H, Lee D and Issadore D 2018 Silicon and glass very large scale microfluidic droplet integration for terascale generation of polymer microparticles *Nat. Commun.* **9** 1222

[24] Nisisako T and Torii T 2008 Microfluidic large-scale integration on a chip for mass production of monodisperse droplets and particles *Lab Chip* **8** 287–93

[25] Amstad E, Chemama M, Eggersdorfer M, Arriaga L R, Brenner M P and Weitz D A 2016 Robust scalable high throughput production of monodisperse drops *Lab Chip* **16** 4163–72

[26] Ofner A, Moore D G, Rühs P A, Schwendimann P, Eggersdorfer M, Amstad E, Weitz D A and Studart A R 2017 High-Throughput Step Emulsification for the Production of Functional Materials Using a Glass Microfluidic Device *Macromol. Chem. Phys.* **218** 1600472

[27] Stolovicki E, Ziblat R and Weitz D A 2017 Throughput enhancement of parallel step emulsifier devices by shear-free and efficient nozzle clearance *Lab Chip* **18** 132–8

[28] Nisisako T, Ando T and Hatsuzawa T 2012 High-volume production of single and compound emulsions in a microfluidic parallelization arrangement coupled with coaxial annular world-to-chip interfaces *Lab Chip* **12** 3426–35

[29] Montessori A, Lauricella M, Succi S, Stolovicki E and Weitz D 2018 Elucidating the mechanism of step emulsification *Phys. Rev. Fluids* **3** 072202

[30] Headen D M, García J R and García A J 2018 Parallel droplet microfluidics for high throughput cell encapsulation and synthetic microgel generation *Microsyst. Nanoeng.* **4** 17076

[31] Tsuda Y, Morimoto Y and Takeuchi S 2010 Monodisperse cell-encapsulating peptide microgel beads for 3D cell culture *Langmuir* **26** 2645–9

[32] Kamperman T, Henke S, Visser C W, Karperien M and Leijten J 2017 Centering Single Cells in Microgels via Delayed Crosslinking Supports Long-Term 3D Culture by Preventing Cell Escape *Small* **13** 1603711

[33] Jeong -H-H, Issadore D and Lee D 2016 Recent developments in scale-up of microfluidic emulsion generation via parallelization *Korean J. Chem. Eng.* **33** 1757–66

[34] Jeong H H, Yadavali S, Issadore D and Lee D 2017 Liter-scale production of uniform gas bubbles via parallelization of flow-focusing generators *Lab Chip* **17** 2667–73

[35] Holtze C *et al* 2008 Biocompatible surfactants for water-in-fluorocarbon emulsions *Lab Chip* **8** 1632–9

[36] Shao F, Yu L, Zhang Y, An C, Zhang H, Zhang Y, Xiong Y and Wang H 2020 Microfluidic Encapsulation of Single Cells by Alginate Microgels Using a Trigger-Gellified Strategy *Front. Bioeng. Biotechnol.* **8** 583065

[37] Zhao X, Liu S, Yildirimer L, Zhao H, Ding R, Wang H, Cui W and Weitz D 2016 Microfluidics-Assisted Osteogenesis:

[38] Vormittag P, Gunn R, Ghorashian S and Veraitch F S 2018 review: a guide to manufacturing car t cell therapies *Curr. Opin. Biotechnol.* **53** 164–81

[39] Utech S, Prodanovic R, Mao A S, Ostafe R, Mooney D J and Weitz D A 2015 Microfluidic Generation of Monodisperse, Structurally Homogeneous Alginate Microgels for Cell Encapsulation and 3D Cell Culture *Adv. Healthcare Mater.* **4** 1628–33

[40] Hati A G, Bassett D C, Ribe J M, Sikorski P, Weitz D A and Stokke B T 2016 Versatile, cell and chip friendly method to gel alginate in microfluidic devices *Lab Chip* **16** 3718–27

[41] Riachy P, Lopez G, Emo M, Stebe M J, Blin J L and Ameduri B 2017 Investigation of a novel fluorinated surfactant-based system for the design of spherical wormhole-like mesoporous silica *J. Colloid Interface Sci.* **487** 310–9

[42] Wagner O, Thiele J, Weinhart M, Mazutis L, Weitz D A, Huck W T and Haag R 2016 Biocompatible fluorinated polyglycerols for droplet microfluidics as an alternative to PEG-based copolymer surfactants *Lab Chip* **16** 65–69

[43] Akartuna I, Aubrecht D M, Kodger T E and Weitz D A 2015 Chemically induced coalescence in droplet-based microfluidics *Lab Chip* **15** 1140–4

[44] Zhang Y *et al* 2021 Microfluidic-templating alginate microgels crosslinked by different metal ions as engineered microenvironment to regulate stem cell behavior for osteogenesis *Mater. Sci. Eng.* C **131** 112497

[45] Cubaud T and Mason T G 2008 Capillary threads and viscous droplets in square microchannels *Phys. Fluids* **20** 053302

[46] Romanowsky M B, Abate A R, Rotem A, Holtze C and Weitz D A 2012 High throughput production of single core double emulsions in a parallelized microfluidic device *Lab Chip* **12** 802–7

[47] Griffin D R, Weaver W M, Scumpia P O, Di Carlo D and Segura T 2015 Accelerated wound healing by injectable microporous gel scaffolds assembled fromannealed building blocks. *Nat. Mater.* **14** 737–44

[48] Liang Y, Zhao X, Hu T, Chen B, Yin Z, Ma P X and Guo B 2019 Adhesive Hemostatic Conducting Injectable Composite Hydrogels with Sustained Drug Release and Photothermal Antibacterial Activity to Promote Full-Thickness Skin Regeneration During Wound Healing *Small* **15** 1900046

[49] Griffin D R *et al* 2020 Activating an adaptive immune response from a hydrogel scaffold imparts regenerative wound healing *Nat. Mater.* **20** 560–9

[50] Zhuang Z, Zhang Y, Sun S, Li Q, Chen K, An C, Wang L, van den Beucken J and Wang H 2020 Control of Matrix Stiffness Using Methacrylate−Gelatin Hydrogels for a Macrophage-Mediated Inflammatory Response *ACS Biomater. Sci. Eng.* **6** 3091–102